Since January 2020 Elsevier has created a COVID-19 resource centre with free information in English and Mandarin on the novel coronavirus COVID-19. The COVID-19 resource centre is hosted on Elsevier Connect, the company's public news and information website.

Biosensors and Bioelectronics 212 (2022) 114379

Contents lists available at ScienceDirect

Biosensors and Bioelectronics

journal homepage: www.elsevier.com/locate/bios

Non-enzymatic signal amplification-powered point-of-care SERS sensor for rapid and ultra-sensitive assay of SARS-CoV-2 RNA

Jingjing Zhang [a,1], Xiaping Miao [b,c,1], Chunyuan Song [a,*], Na Chen [b], Jingrong Xiong [a], Hongyu Gan [a], Jie Ni [a], Yunfeng Zhu [a], Kaiting Cheng [b,c,**], Lianhui Wang [a,***]

[a] State Key Laboratory for Organic Electronics and Information Displays & Jiangsu Key Laboratory for Biosensors, Institute of Advanced Materials (IAM), Jiangsu National Synergetic Innovation Center for Advanced Materials (SICAM), Nanjing University of Posts & Telecommunications, Nanjing, 210023, China
[b] Guangzhou KingMed Center for Clinical Laboratory Co., Ltd, 10 Luoxuan 3rd Road, Guangzhou International Biotech Island, Guangdong, 510005, Guangdong, China
[c] Guangzhou Laboratory, No.9 XingDaoHuanBei Road, Guangzhou International Bio Island, Guangzhou, 510005, Guangdong Province, China

ARTICLE INFO

Keywords:
SERS
COVID-19
SARS-CoV-2 RNA
Target recycling signal amplification
Early detection

ABSTRACT

The development of rapid and ultra-sensitive detection technology of SARS-CoV-2 RNA for shortening the diagnostic window and achieving early detection of virus infections is a huge challenge to the efficient prevention and control of COVID-19. Herein, a novel ultra-sensitive surface-enhanced Raman spectroscopy (SERS) sensor powered by non-enzymatic signal amplification is proposed for rapid and reliable assay of SARS-CoV-2 RNA based on SERS-active silver nanorods (AgNRs) sensing chips and a specially designed smart unlocking-mediated target recycling signal amplification strategy. The SERS sensing was carried out by a one-pot hybridization of the lock probes (LPs), hairpin DNAs and SERS tags with SARS-CoV-2 RNA samples on an arrayed SERS sensing chip to achieve the recognition of SARS-CoV-2 RNA, the execution of nuclease-free unlocking-mediated target recycling signal amplification, and the combination of SERS tags to generate SERS signal. The SERS sensor for SARS-CoV-2 RNA can be achieved within 50 min with an ultra-high sensitivity low to 51.38 copies/mL, and has good selectivity in discriminating SARS-CoV-2 RNA against other respiratory viruses in representative clinical samples, which is well adapted for rapid, ultra-sensitive, multi-channel and point-of-care testing of viral nucleic acids, and is expected to achieve detection of SARS-CoV-2 infection in earlier detection windows for efficient COVID-19 prevention and control.

1. Introduction

The ongoing Coronavirus Disease 2019 (COVID-19) pandemic caused by the novel severe acute respiratory syndrome coronavirus 2 (SARS-CoV-2) is a huge threat worldwide (Bchetnia et al., 2020; Sohrabi et al., 2020; Wu, A. et al., 2020; Wu, F. et al., 2020). The main way to efficiently prevent and control the epidemic is the rapid and accurate identification of virus at an early stage, especially in the areas that have no effective drugs and vaccines yet (Aydogdu et al., 2022; Liu, C. et al., 2020; Udugama et al., 2020). The molecular diagnosis of characteristic nucleic acid of SARS-CoV-2 single-stranded positive-sense RNA genome swabbed from a patient's throat or nasal cavity has been adopted to achieve the early detection of the viral infection or contamination (Chen et al., 2020; Wu, A. et al., 2020; Wu, F. et al., 2020), but the great challenge of early identification of COVID-19 is how to detect extremely trace amount of SARS-CoV-2 RNA from complex samples. Currently, the traditional detection methods are developed based on the enzyme-related nucleic acid amplifications such as polymerase chain reaction (PCR) (Bienko et al., 2013; Chang et al., 2020; Corman et al., 2020; Karami et al., 2021; Markou et al., 2008; Sharfstein et al., 2020; Smyrlaki et al., 2020), loop-mediated isothermal amplification (LAMP) (Nguyen and Lee, 2021; Yin et al., 2021; Zhu et al., 2020), and recombinase polymerase amplification (RPA) (Cherkaoui et al., 2021; De Felice et al., 2022; Mancuso et al., 2021). Despite the great success of

* Corresponding author.,
** Corresponding author. Guangzhou KingMed Center for Clinical Laboratory Co., Ltd, 10 Luoxuan 3rd Road, Guangzhou International Biotech Island, Guangdong, 510005, Guangdong, China.
*** Corresponding author.
E-mail addresses: iamcysong@njupt.edu.cn (C. Song), zb-chengkeding@kingmed.com.cn (K. Cheng), iamlhwang@njupt.edu.cn (L. Wang).
[1] These authors contributed equally.

https://doi.org/10.1016/j.bios.2022.114379
Received 7 January 2022; Received in revised form 12 April 2022; Accepted 13 May 2022
Available online 16 May 2022

these techniques in trace viral nucleic acid testing, especially the PCR as the "gold standard" in SARS-CoV-2 diagnostics, there are still significant deficiencies or limitations in the requirements of precise primer design, enzyme activity-dependence, fine thermal control, and complex operations (Liu, R. et al., 2020; Wang et al., 2011). These liabilities make the detection expensive and time-consuming (i.e., each operation takes approximately 4 h and the average turnaround time for test results is 24–72 h) (Hwang et al., 2021; Klein, 2002), and lead to a risk of carry-over contamination causing false positives. Critically, the long testing backlog is distinctly unpredictable for the fast spread of COVID-19 in a short period of time, and the earlier detection is limited by the sensitivity of the commercial fluorescent PCR assays with generally high limit of detections (LODs, >200 copies/mL) (Mahapatra and Chandra, 2020; Perez-Lopez and Mir, 2021). Therefore, the development of novel ultra-sensitive detection methods and point-of-care sensors for achieving rapid and reliable molecular diagnosis of ultra-low analyte in earlier detection window is significantly important.

Compared to the traditional fluorescent analysis and PCR-based enzyme-related nucleic acid amplification strategies, the enzyme-free signal amplifications without the time-consuming complex process of nucleic acid amplification, as well as the surface-enhanced Raman spectroscopy (SERS) analysis with single-molecule sensitivity, are expected to provide the possible solutions for fast, ultra-sensitive detection to meet the tough requirement of viral infection assay in an earlier detection window. As a representative enzyme-free isothermal target recycling signal amplification strategy, the catalytic hairpin assembly (CHA), being initiated by cyclical opening of hairpin 1 (H1) and hairpin 2 (H2) when the target exists, and forming numerous H1–H2 duplexes and recycling the target (Peng et al., 2020; Wu et al., 2021; Yin et al., 2008), can generate obvious signal amplification without amplifying the target nucleic acid, and is known as a simple, robust and efficient amplification method without complicated enzyme reactions and time consuming processes. Moreover, SERS is a Raman signal amplification technique derived from the localized surface plasmon resonance (LSPR) with the signal enhanced generally 10^5-10^8 and extremely 10^{15} folds (Hossain et al., 2008; Lee et al., 2011; Nie and Emory, 1997; Sharma et al., 2012), which is considered as a powerful tool for achieving ultra-sensitive biodetections of microliter samples. So far, the SARS-CoV-2 RNA detection technology based on SERS analysis is still very limited, and the sensitive and convenient detection strategies satisfied the fast and on-site tests are particularly needed for epidemic prevention and control.

To develop robust device for achieving reliable and efficient detection of SARS-CoV-2 RNA in the earlier infection, the ideal SERS sensors should have the following characteristics: (1) ultra-sensitivity with the LOD less than 200 copies/mL; (2) rapid detection with the detection time significantly shorter than the PCR assays; (3) point-of-care testing with good convenience and practicality. Therefore, we need to design smart enzyme-free signal amplification strategy based on the SERS detection technique to achieve high specific recognition of SARS-CoV-2 single-stranded positive-sense RNAs and efficient target-triggered CHA-based signal amplification, as well as the effective capture of SERS tags by a one-pot incubation. In this work, a novel SERS sensor for rapid, ultra-sensitive and reliable SARS-CoV-2 RNA detection was proposed based on portable SERS-active silver nanorods (AgNRs) sensing chips and a one-pot CHA-based nuclease-free signal amplification strategy. The SERS sensor includes AgNRs SERS sensing chip (i.e., MCH-blocked capture ssDNAs (C)-modified AgNRs) with arrayed sensing wells, SERS tags (i.e., gold nanoparticles (AuNPs) co-labeled with probe ssDNAs (P) and Raman molecules), the lock probes (LPs) for recognizing SARS-CoV-2 RNA, and the hairpin DNAs for conducting CHA-based target recycling amplifications. The assay was carried out by a one-pot incubation of lock probes (LPs), hairpin DNAs, SERS tags with analyte in SERS sensing chip wells, followed by SERS measurements via a portable Raman spectrometer. The optimal sensing strategy was built by systematically investigating the high-yield preparation of lock probes (LPs), the optimal SERS sensing chip with preferred capture ssDNAs immobilization and MCH blocking, and the appropriate detection time. The performance of SERS sensor on sensing SARS-CoV-2 RNA by a portable Raman spectrometer was studied, and the SERS assay has ultra-sensitivity for the detection of SARS-CoV-2 RNA and good selectivity in discriminating SARS-CoV-2 RNA against other respiratory diseases in representative clinical samples, which is well adapted for rapid, ultra-sensitive, multi-channel and point-of-care testing of viral nucleic acids in earlier detection window of SARS-CoV-2 infection.

2. Experimental section

2.1. Reagents and materials

All single-stranded DNAs (ssDNAs) used in this work and the characteristic DNA fragment (62 nucleotides) of SARS-CoV-2 in the ORF1ab gene region corresponding to nucleotides 13342–13403 (NCBI Reference Sequence: NC_045512.2) were artificially synthesized by TaKaRa Biotech Co., Ltd. (Dalian, China), and their sequences were listed in Table S1. The characteristic DNA fragment of SARS-CoV-2 (target DNA, T) was used for the characterization and optimization of the sensing strategy. The test samples such as SARS-CoV-2 RNA control (TEST08), Influenza A virus (H1N1) RNA control (CA0758) and Influenza B virus (Victoria) RNA control (CA0759) were purchased from GeneWell Technology (Shenzhen) Co., LTD (Shenzhen, China). Rhinovirus control (RVMQC) was obtained from Qnostics (Glasgow, UK), consisting of 5 × 1 mL samples of a medium containing whole Rhinovirus. The other clinical samples including Respiratory syncytial virus (RSV) and Adenovirus (Adeno) RNA samples were collected and extracted by Guangzhou KingMed Center for Clinical Laboratory (Guangzhou, China). All the nucleic acid of Rhinovirus control and clinical samples were extracted by FastPure Viral DNA/RNA Mini Kit (Nanjing Vazyme Medical Technology Co., Ltd). Briefly, aliquot 500 μL of lysis solution was added to a 1.5 mL of RNase-free tube containing 200 μL of clinical sample. After mixing thoroughly, the mixtures were transferred to an adsorption column placed in a 2 mL of collection tube and centrifuged at 12,000×*g* for 1 min. The adsorption column was then washed by washing buffer twice (i.e., by adding 600 μL washing buffer to the adsorption column and centrifuging at 12,000×*g* for 30 s). The empty adsorption column was placed in the collection tube and centrifuged at 12,000×*g* for 2 min. The adsorption column was then transferred to a new collection tube, followed by adding 50 μL of elution buffer. The mixtures were incubated at room temperature for 1 min, and then centrifuged at 12,000×*g* for 1 min. Finally, the eluted DNA/RNAs were stored at −20 °C for short-term storage, or stored at −70 °C for long-term storage. The study of clinical samples was approved by the Medical Ethical Committee of the Guangzhou KingMed Center for Clinical Laboratory (2021015). All ssDNAs and RNA samples were dissolved and diluted with diethyl pyrocarbonate (DEPC) water (Sangon Biotech Co., Ltd. (Shanghai, China)) to avoid the degradation of RNA during the detection. Gold nanoparticles (AuNPs, 30 nm in diameter) were bought from British Biocell International (Cardiff, UK). Tris (2-carboxyethyl) phosphine (TCEP), 5,5′-Dithiobis (2-nitrobenzoic acid) (DTNB, 99%), and mercaptohexanol (MCH) were purchased from Sigma-Aldrich (Shanghai, China). TM buffer (10 mM Tris, and 25 mM $MgCl_2$, pH 8.0) was used for DNA hybridization, and 5 × TBE buffer (445 mM Tris, 10 mM EDTA-2Na, and 450 mM H_3BO_3) was used to prepare SERS tags. All solutions were prepared with Millipore ultrapure water (18.2 MΩ cm) and autoclaved before use. The SERS-active silver nanorods (AgNRs) array substrates were fabricated according to the procedure described in our previous works (Song et al., 2014, 2016, 2020b; Zhang et al., 2019), and arrayed sensing wells (3 × 10, 4 mm in diameter and 1 mm in height of each well) on the AgNRs substrate were obtained by molding well arrayed premopolydimethylsiloxane (PDMS) film. Fig. S1 shows the SEM image of AgNRs array and a photo of the PDMS wells-patterned AgNRs substrate.

2.2. Characterizations and Apparatuses

The UV–vis absorption spectra were recorded by a UV-3600 UV–vis spectrophotometer (Shimadzu, Japan). The transmission electron microscopy (TEM) images were taken by a HT7700 TEM (Hitachi, Japan), and scanning electron microscopy (SEM) images were captured by a S-4800 field-emission SEM (Hitachi, Japan). The dynamic light scattering (DLS) and zeta potential were conducted by a zeta potential analyzer (Brookhaven, America). The 10% native polyacrylamide gel electrophoresis (PAGE) was operated on a Bio-Rad electrophoretic apparatus (BIO-RAD Laboratories, USA) at 80 V for 90 min. The fluorescence spectra from 597 to 700 nm were collected by a RF-5301PC fluorescence spectrophotometer (Shimadzu, Japan) with 5 nm excitation and emission slits. The SERS spectra were measured by an i-Raman® portable Raman spectrometer (B&W Tek, USA), with a 785 nm excitation wavelength, 5% laser power, 1 s exposure time and 1 time accumulation. Unless otherwise specified, 10 spectra from different spots in each well were recorded to obtain an averaged SERS spectrum from each sample.

2.3. Preparation of SERS tags

The SERS tags were prepared by immobilizing thiolated probe DNAs and Raman molecules on the surface of AuNPs through Au–S covalent bonds, as shown in Scheme 1a. Briefly, 10 μL of 50 μM probe DNA (P), 500 μL of 0.33 nM AuNPs and 50 μL of 5 × TBE buffer were mixed together under continuous shaking. After incubation for 5 h, 5, 10, 15 and 20 μL of 2 M NaCl solutions were added into the above mixture every 30 min in sequence to age the P-labeled AuNPs for at least 5 h. After that, 10 μL of 100 μM Raman molecules DTNB was added in the mixture and incubated at 25 °C for 3 h, and the final solution was then washed with 0.5 × TBE and centrifuged (6000 rpm for 20 min) three times. The SERS tags were obtained by re-dispersing the sediments in 50 μL of DEPC-treated 0.5 × TBE and stored in a 4 °C refrigerator for further usage. The SERS tags were characterized by TEM, UV–vis absorption, zeta potential, DLS, and SERS. The Raman band of DTNB at 1331 cm^{-1} was selected as the characteristic peak for SERS analysis.

2.4. Preparation of the lock probes (LPs) and SERS sensing chip

As shown in Scheme 1b, the lock probes (LPs) were prepared by incubation primer DNA with hairpin DNA H1 (H1), i.e., 10 μL of 50 μM primer DNA and 10 μL of 50 μM H1 were mixed in TM buffer, followed by an anneal treatment (i.e., heating at 95 °C for 5 min and then cooled down to room temperature). The LPs were then diluted to 5 μM by TM buffer for further usage. For preparing SERS sensing chip, the PDMS-well patterned AgNRs substrate was rinsed with DEPC water and TM buffer in sequence. Afterwards, 20 μL of 500 nM capture DNA (C) was dropped in each well and incubated for 3 h at 37 °C to immobilize C onto the AgNRs by Ag–S bonds. After TM buffer wash, 20 μL of 1 mM MCH solution was incubated in each well to block the C-uncovered region for 10 min to avoid nonspecific adsorption. The SERS sensing chip was obtained after TM buffer washing three times.

2.5. SERS sensing protocol

A one-step protocol was conducted for SERS detecting SARS-CoV-2 RNA, i.e., 4 μL of 5 μM LP, 4 μL of 10 μM hairpin DNA H2 (H2), 10 μL of 3.3 nM SERS tags, and 2 μL of analyte with a certain concentration were mixed together in each well on the SERS sensing chip and incubated for 50 min at 37 °C under shaking. Finally, the SERS measurements at 10 spots of each well were performed after DEPC water washing three times and then air-dry. For obtaining the concentration-dependent SERS assay, the SARS-CoV-2 RNA control was diluted to different concentrations, i.e., 10^2, 10^3, 5×10^3, 10^4, 10^5 and 10^6 copies/mL, followed by the one-step SERS assay. For characterizing the specificity of the SERS strategy, specific positive samples (10^3 and 10^6 copies/mL SARS-CoV-2 RNA control) and unspecific negative control (Influenza A (10^6 copies/mL), Influenza B (10^6 copies/mL), Rhinovirus RNAs (10^6

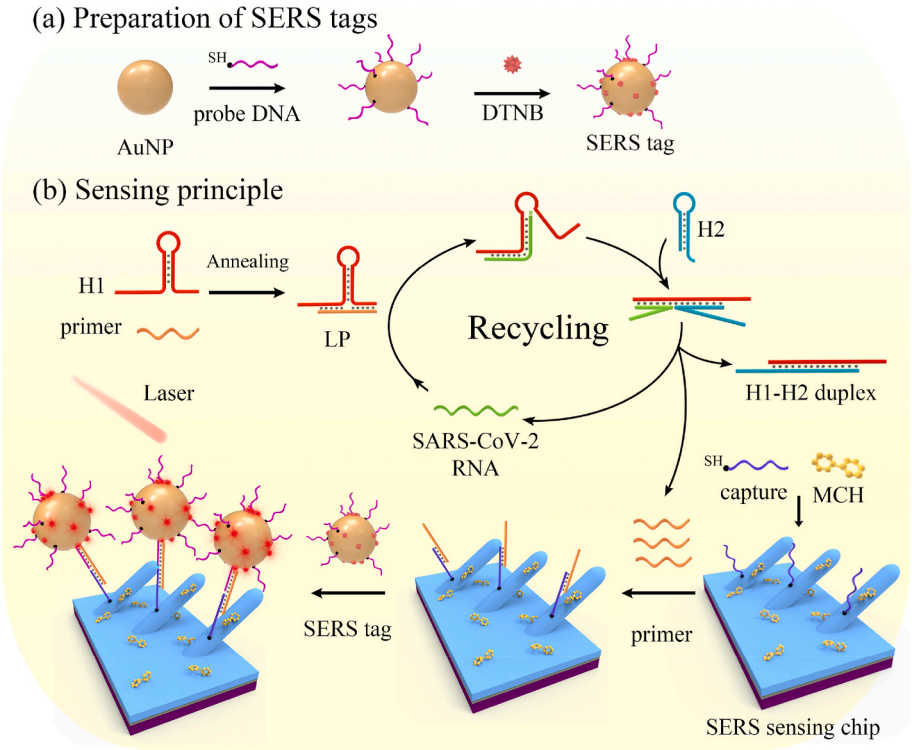

Scheme 1. Schematic illustrations of (a) the preparation of SERS tags and (b) the unlocking-mediated target recycling signal amplification strategy for SERS detection of SARS-CoV-2 RNA.

copies/mL), and artificially extracted Respiratory syncytial virus (RSV) and Adenovirus (Adeno) RNAs), as well as the blank control were tested by SERS assay.

3. Results and discussion

3.1. Sensing principle and feasibility of unlocking-mediated target recycling signal amplification strategy

For high sensitive and specific detection of SARS-CoV-2 RNA, the wildly-agreed gene fragment in the open reading frame 1 ab (ORF1ab) region with highly conserved viral nucleic acid sequences was selected as the target sequence (Li et al., 2021; Udugama et al., 2020; Wang et al., 2021). Scheme 1b illustrates the unlocking-mediated target recycling signal amplification strategy for SERS detection of SARS-CoV-2 RNA, which includes five parts, i.e., LPs, H2, SERS tags, SERS sensing chip and analyte. The primer DNA can hybridize with a hairpin DNA H1 via the complementary bases marked in the same blue and purple colors (Table S1) to form a lock probe (LP). In the presence of SARS-CoV-2 RNA, the toehold-mediated hybridization between H1 and the complementary sequence of SARS-CoV-2 RNA occurs, which makes the LP partially open, and with the aid of fuel hairpin DNA H2, the SARS-CoV-2 RNA and previous locked primer in LP are released due to the competitive hybridization between H1 and H2 to form a H1–H2 duplex. Therefore, the released SARS-CoV-2 RNA can further be reused to trigger the next unlocking of LPs, and as a result many primers are unlocked from the LPs. These released primers can be captured by SERS sensing chip via the specific hybridization with C, and the SERS tags can further be trapped by the primers on the chip. Finally, the SERS signal from the chip is collected for sensitive assay of SARS-CoV-2 RNA.

The theoretical calculations of the hybridization efficiency of the DNAs were done by the Unpack Analysis to make sure the reasonable design of the CHA-based non-enzymatic signal amplification strategy. The LPs can be assembled in high-yield (~99%) (Fig. S2a) and in the mixture of the target DNAs (T), LPs and the fuel hairpin DNAs H2, the T can be efficiently released (~96%) and nearly 63% of the primer can fall off of the LPs since the formation of the H1–H2 duplex (Fig. S2b). In fact, the release efficiency of primer is acctually high in the T-triggered CHA reactions, which is confirmed by the grayscale analysis (Fig. S2c), i.e., the release efficiencies of T and primer reach 91.5% (529.3/570.16) and 96.0% (2781.4/2898.6), respectively. These theoretical analyses indicate that efficient CHA-based non-enzymatic signal amplification can be achieved. Moreover, it should be noted that, under the excitation of 785 nm laser, there are not only localized electromagnetic fields (EM) around the AuNPs but also EM coupling between the AgNR and AuNPs (Fig. S3) (Yang et al., 2022), which can produce strong SERS enhancement to achieve sensitive detections.

Fig. 1 shows the PAGE pattern for characterizing the unlocking-mediated target recycling amplification. The lanes 1 to 4 illustrate the electrophoresis strips of primer, target DNA (T), H1, and H2, respectively. Due to the high-yield formation of LPs, an obvious strip of LPs with lower migration rate relative to the individual primer (lane 1) or H1 (lane 3) is observed. When the T was mixed with the LPs, a new slowly moved hybrid strip differing from the primer, H1 and T is found in lane 6, which indicates that the T hybridized with H1 and triggered the partially opening of H1. Furthermore, by adding fuel hairpin DNA H2, a bright strip of DNA duplexes of H1 and H2 is observed in lane 7 together with two very light strips of T and primer according to the strips shown in lanes 1 and 2. It should be noted that the LPs cannot be opened without the trigger of T as shown in lane 8, and the H1 and H2 with hairpin structures can protect them from co-hybridization without external trigger (lane 9). These results confirm that the recycling amplifications of T and primer can be effectively achieved by the proposed unlocking-mediated target-trigged recycling amplifications.

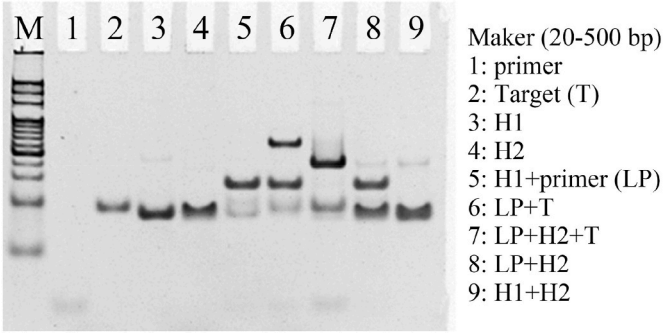

Fig. 1. PAGE analysis of the unlocking-mediated target recycling amplification. Marker (20–500 bp), lane 1: primer, lane 2: target DNA (T), lane 3: H1, lane 4: H2, lane 5: H1+primer (i.e., LP), lane 6: LP + T, lane 7: LP + H2+T, lane 8: LP + H2, lane 9: H1+H2.

3.2. Characterization of SERS tags

Fig. S4 shows the characterizations of the SERS tags which are fabricated by modifying probe DNAs (P) and Raman molecules DTNB on the surface of AuNPs in sequence. The TEM images shown in Figs. S4a and b indicate that the AuNPs with an average diameter of 30 nm are monodisperse, and there is no obvious morphology change after the co-immobilization of P and DTNB (i.e., SERS tags). The evolutions of absorption peak (Fig. S4c), zeta potential (Fig. S4d), and DLS hydrodynamic diameter (Fig. S4e) of AuNPs after the modifications of P and DTNB in sequence confirm the successful construction of the SERS tags. Fig. S4f shows the representative SERS spectrum of DTNB collected from the SERS tags, which confirms that the bright SERS tags are suitable for SERS detections.

3.3. Optimal sensing conditions

To establish the optimal sensing strategy, the sensing conditions were explored systematically, including the concentration ratios of primer and H1 for preparing LPs in high-yield, the immobilization concentration of C on AgNRs for obtaining sensitive SERS sensing chip, the MCH blocking time for avoiding unspecific absorption, and the detection time for achieving time-saving test.

Fig. S5a shows the fluorescence spectra of LPs assembled by mixing different molar ratios of primer-ROX (i.e., ROX-labeled primer, Table S1) and H1-BHQ (i.e., fluorescence quencher BHQ2-labeled H1), i.e., 1:0 (without H1), 1:0.8, 1:1, 1:1.25, 1:1.5, and 1:2, and the corresponding fluorescence intensities of ROX at 603 nm were plotted in Fig. S5b. As the dosage of H1 increases, the fluorescence intensity decreases continuously until it reaches a minimum value when the ratio is 1:1.25, which means that the excessive molecules of H1 relative to the primer can obtain a high yield of LPs in which the primers are locked in LPs. Furthermore, the SERS characterizations shown in Figs. 2a and S6a indicate that the best SERS sensing of 10 fM and 10 pM targets are obtained when the molar ratio is 1:1. Considering that the excessive molecules of H1 (i.e., the free H1 rather than the trapped H1 in LPs) can hybridize with the target without the release of primer for further SERS detection, which may reduce the cycling amplification efficiency, the optimal molar ratio of primer and H1 for preparing LPs is determined as 1:1.

The optimal concentration of C for preparing SERS sensing chip was investigated by modifying the AgNRs with different concentrations of C to detect 10 pM target DNA, respectively. The result shown in Figs. 2b and S6b illustrate that the SERS sensing signal increases with the increasing immobilization concentration of C, and the optimal immobilization concentration of C is determined as 500 nM since a saturate point is observed.

Fig. 2c shows the study on MCH blocking for minimizing the nonspecific adsorption. The AgNRs were blocked by 20 μL of 1 mM MCH

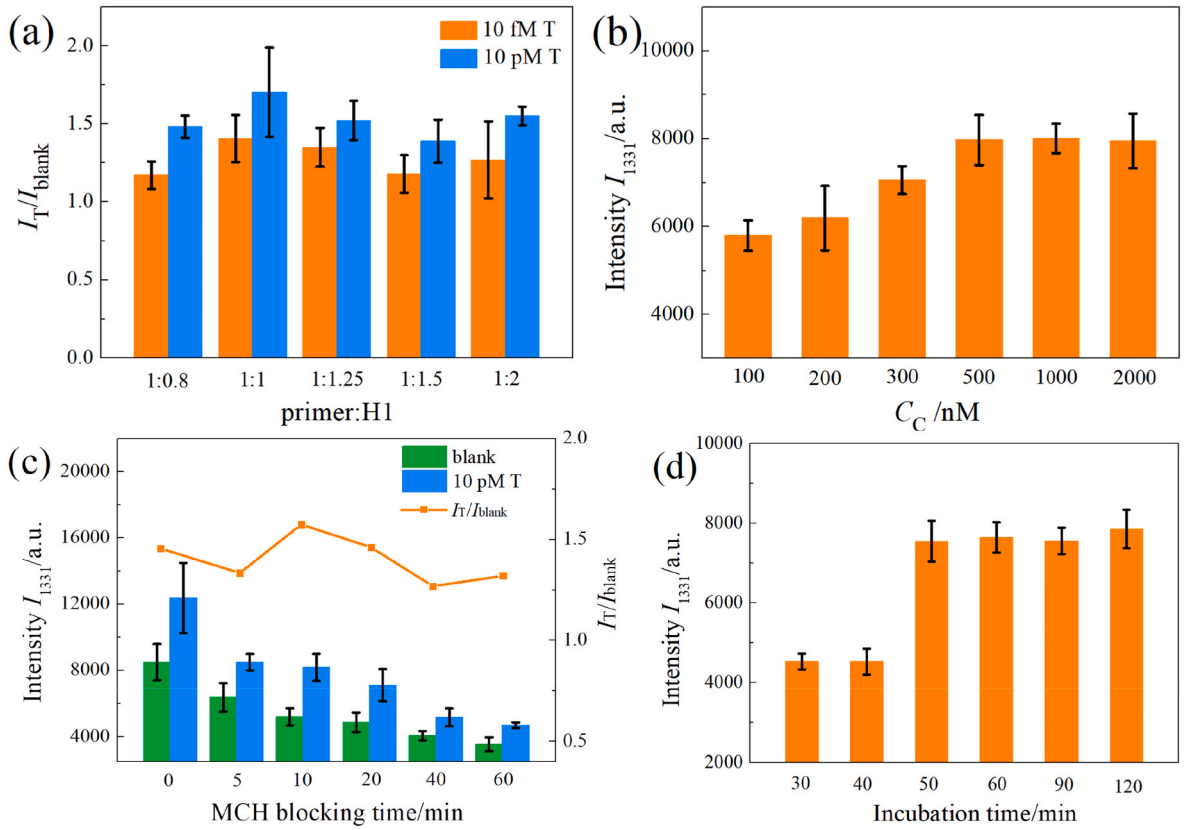

Fig. 2. Optimization of the sensing conditions. (a) Plot of the SERS sensing results of 10 fM and 10 pM target DNAs obtained by using the LPs prepared with different molar ratios of primer and H1 (i.e., 1:0 (without H1), 1:0.8, 1:1, 1:1.25, 1:1.5, and 1:2). (b) Plot of SERS sensing results collected from the SERS sensing chips prepared by modifying the AgNRs with different concentrations of C (i.e., from 100 to 2000 nM). (c) Plot of sensing results obtained from the SERS sensing chips blocked by MCH for different blocking times from 0 to 60 min. (d) Plot of SERS sensing results of target DNA with different incubation times from 30 to 120 min. Unless otherwise specified the concentration of target DNA was 10 pM.

for different times, i.e., 0, 5, 10, 20, 40, and 60 min, respectively. The maximum signal-to-noise ratio (I_T/I_{blank}) for testing 10 pM target DNA is achieved from the SERS sensing chip blocked for 10 min, i.e., the optimal MCH blocking time is 10 min.

Fig. S6c illustrates the SERS study on the optimal detection time, which was investigated by adjusting the incubation time of the mixtures including 10 pM target DNA in the sensing wells from 30 to 120 min respectively, and according to the data plotted in Fig. 2d, the optimal SERS signal is obtained from the assay after incubation for 50 min, i.e., the best detection time is 50 min.

3.4. Performance of SERS sensor on detection of SARS-CoV-2 RNA

Fig. 3a shows the concentration-dependent SERS assay spectra of SARS-CoV-2 RNA control. The SERS signal is enhanced with the increasing concentration of SARS-CoV-2 RNA control, which is also confirmed by characterizing the specifically captured SERS tags on the SERS sensing chip. The SEM images shown in Fig. 3c–i illustrate the AuNPs captured on the AgNRs arrays in the presence of SARS-CoV-2 RNA control with different concentrations, which indicates that monolayers of AuNPs were absorbed on the AgNRs arrays and the density of AuNPs increases with the concentration of SARS-CoV-2 RNA control from 35 ± 4 particles/μm^2 of 10^2 copies/mL to 104 ± 4 particles/μm^2 of 10^6 copies/mL (Fig. S7), resulting in the enhanced SERS signal. The signal-to-noise ratio (I_T/I_{blank}) of SERS peak at 1331 cm^{-1} plotted in Fig. 3b follows a linear relationship ($I_T/I_{blank} = 0.17 \times \mathrm{Log}C_T + 0.75$, $R^2 = 0.980$) with the logarithm concentration of SARS-CoV-2 RNA control in the range from 10^2 to 10^6 copies/mL, and the limit of detection (LOD) was evaluated to be 51.38 copies/mL according to the definition that the LOD gives a I_T/I_{blank} difference larger than three times the standard deviation of the blank signal (Fan et al., 2021; Song et al., 2020a). These results indicate that the proposed SERS strategy has a wide linear detection range and an ultra-low LOD for SARS-CoV-2 RNA detection, which is much more sensitive than the other reported methods summarized in Table S2.

Fig. 4 shows the specificity characterization results of the SERS sensing. According to the SERS spectra shown in Fig. 4a and the corresponding I_T/I_{blank} data plotted in Fig. 4b, the proposed SERS strategy exhibits negative SERS responses to the Influenza A (H1N1), Influenza B, Respiratory syncytial virus, Adenovirus, and Rhinovirus RNAs, and the signals of negative samples are submerged in the background (blank), while the positive samples generate obviously stronger SERS signal with respect to the blank. The SEM images of the AuNPs captured on the AgNRs arrays after the negative and positive assays are shown in Figs. S8a–h, and the densities of AuNPs plotted in Fig. S8i indicate that distinct AuNPs were captured by the positive samples (i.e. 104 ± 4 particles/μm^2 of 10^6 copies/mL and 46 ± 2 particles/μm^2 of 10^3 copies/mL), while very low-density of AuNPs (ranging from 11 ± 1 to 28 ± 3 particles/μm^2) were observed on AgNRs arrays after the tests of blank control and negative samples, which is consistent with the sensing results of SERS. These characteristics show the good selectivity of the proposed ultra-sensitive SERS strategy for the reliable detection of SARS-CoV-2 RNA.

3.5. Uniformity and stability of the SERS sensing

Fig. 5a shows the I_T/I_{blank} values of the measurements recorded at 20 random spots in each well for detecting 0, 10^3, and 10^6 copies/mL SARS-

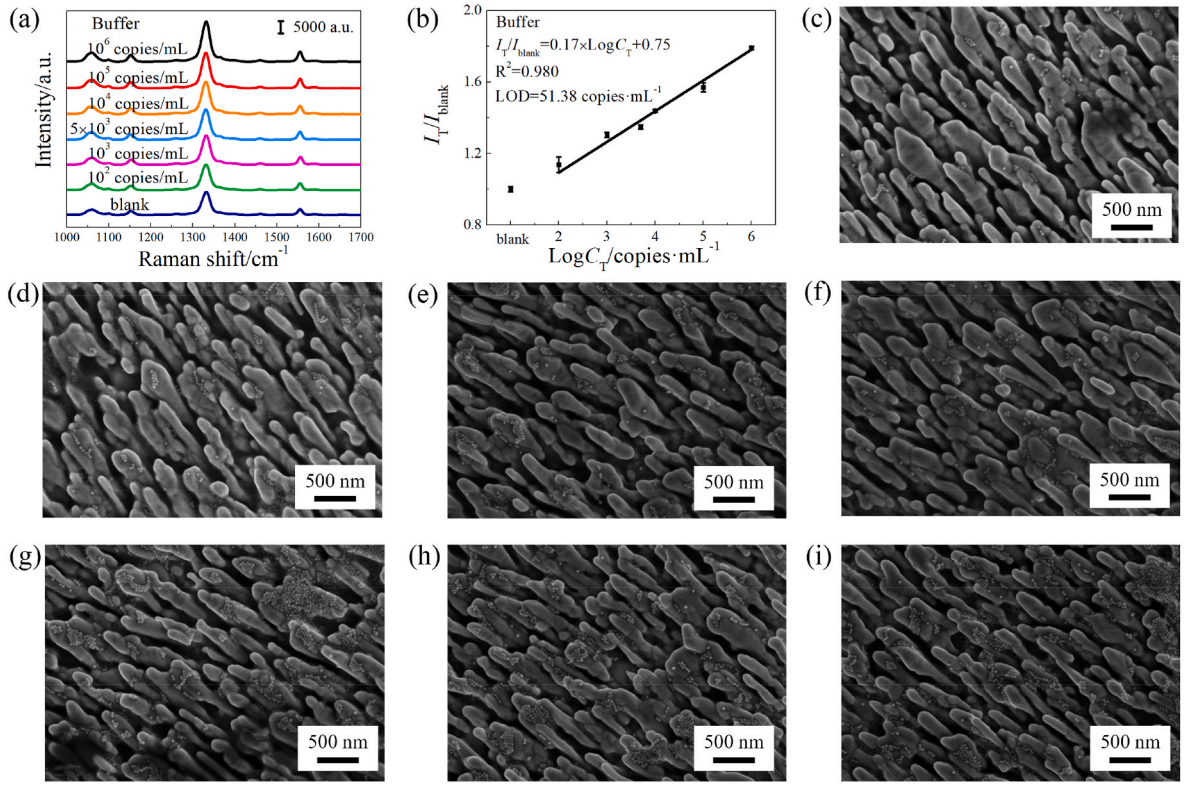

Fig. 3. Sensitivity of the SERS sensing of SARS-CoV-2 RNA. (a) Concentration-dependent SERS assays spectra, i.e., 0 (blank control), 10^2, 10^3, 5×10^3, 10^4, 10^5, and 10^6 copies/mL. (b) Plot of linear relationship fitted between I_T/I_{blank} and the logarithm concentration of SARS-CoV-2 RNA in the range from 10^2 to 10^6 copies/mL. Error bars show the standard deviations of 10 measurements. (c–i) SEM images of the AuNPs captured on the AgNRs arrays after the assays of SARS-CoV-2 RNA with different concentrations: (c) 0 (blank), (d) 10^2, (e) 10^3, (f) 5×10^3, (g) 10^4, (h) 10^5, and (i) 10^6 copies/mL.

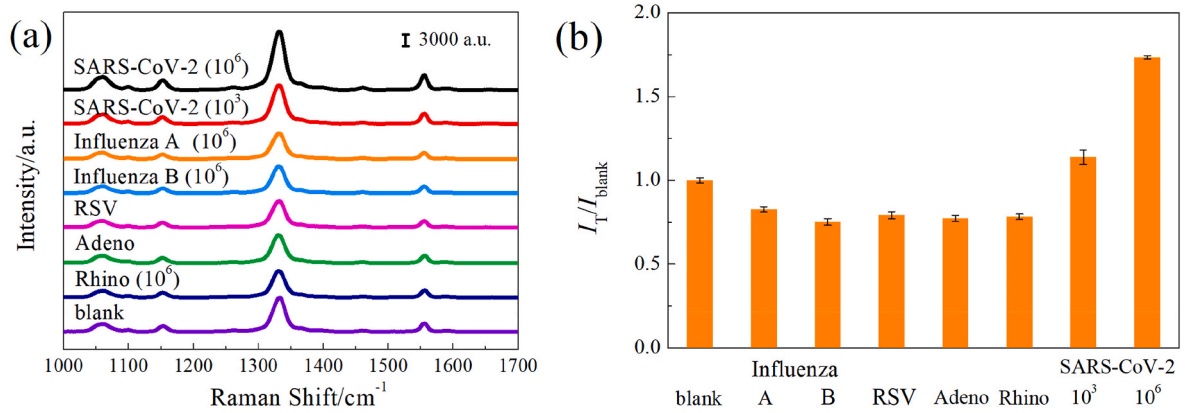

Fig. 4. Specificity characterization of the SERS sensing. (a) SERS spectra of the detection of positive SARS-CoV-2 RNA (10^3 and 10^6 copies/mL), and negative samples (i.e., Influenza A (10^6 copies/mL), Influenza B (10^6 copies/mL), Rhinovirus (Rhino, 10^6 copies/mL), Respiratory syncytial virus (RSV) and Adenovirus (Adeno) RNAs), as well as the blank control. (b) Plots of I_T/I_{blank} values corresponding to the SERS spectra shown in (a).

CoV-2 RNA, respectively. The I_T/I_{blank} at 1331 cm^{-1} have no obvious fluctuations with relative standard derivations (RSDs) $\leq$ 7.71%, which were within the acceptable range. Moreover, the I_T/I_{blank} values obtained from three batches of SERS detection of the positive, negative and blank samples illustrate that the sensing results are consistent between the different batches, which indicates the good uniformity and stability of the SERS sensing for testing SARS-CoV-2 RNA.

4. Conclusions

In summary, a novel non-enzymatic signal amplification-powered point-of-care SERS sensor for rapid, ultra-sensitive and reliable assay of SARS-CoV-2 RNA was proposed based on SERS-active AgNRs sensing chips and a smart unlocking-mediated target recycling signal amplification strategy. The SERS sensing was carried out by a one-pot hybridization of the lock probes (LPs), hairpin DNAs and SERS tags with SARS-CoV-2 RNA samples on an arrayed SERS sensing chip to achieve the recognition of SARS-CoV-2 RNA, execution of nuclease-free unlocking-mediated target recycling signal amplification, and combination of SERS tags. The lock probes (LPs) can be specifically recognized and unlocked by SARS-CoV-2 RNAs, and then with the help of fuel hairpin DNAs CHA-based target recycling amplifications were triggered, which results in the enhanced capture of SERS tags on the SERS sensing chip to generate strong SERS signal for ultra-sensitive detection of SARS-CoV-2 RNA. The

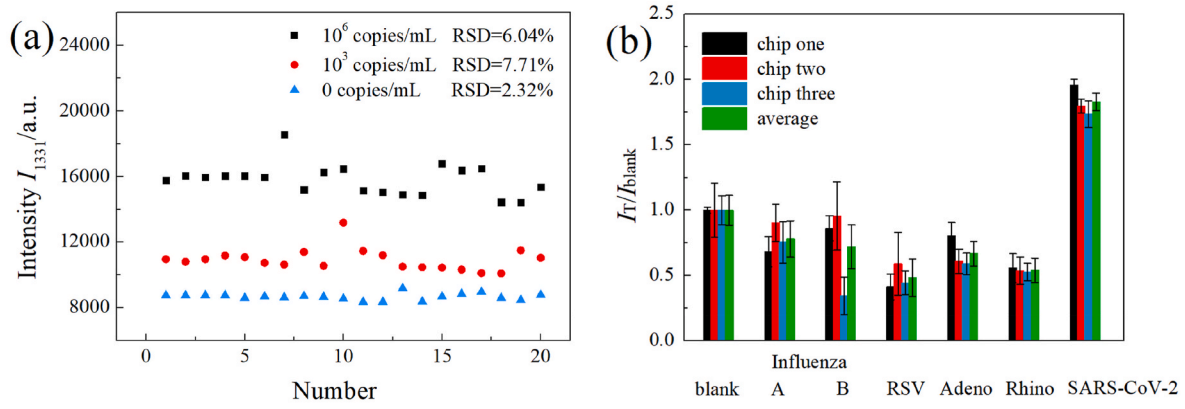

Fig. 5. Uniformity and stability analyses of the SERS sensing. (a) Plot of SERS intensities at 1331 cm^{-1} collected from 20 random spots in each well on the AgNRs for detecting 0, 10^3 and 10^6 copies/mL SARS-CoV-2 RNA. (b) Plot of I_T/I_{blank} at 1331 cm^{-1} obtained from three batches of SERS detection of the positive (10^6 copies/mL), negative (Influenza A (10^6 copies/mL), Influenza B (10^6 copies/mL), Rhinovirus (Rhino, 10^6 copies/mL), Respiratory syncytial virus (RSV), and Adenovirus (Adeno) RNAs and blank samples.

proposed SERS sensor for SARS-CoV-2 RNA can be achieved within 50 min and provides a wide linear detection range from 10^2 to 10^6 copies/mL with the LOD low to 51.38 copies/mL, and shows good detection uniformity and stability, as well as good selectivity in discriminating SARS-CoV-2 RNA against other respiratory viruses. The good performance of the SERS sensors on SARS-CoV-2 RNA detection confirms the significant advantages in terms of ultra-sensitivity, rapid detection, and point-of-care testing, which makes them well adapted for reliable and convenient detection of viral nucleic acids, and is expected to achieve early detection of virus infections for efficient COVID-19 prevention and control.

CRediT authorship contribution statement

Jingjing Zhang: Methodology, Investigation, Formal analysis, Writing – original draft. **Xiaping Miao:** Investigation, Formal analysis, Validation, Writing – review & editing. **Chunyuan Song:** Conceptualization, Methodology, Writing – review & editing, Supervision. **Na Chen:** Investigation, Formal analysis. **Jingrong Xiong:** Investigation, Validation. **Hongyu Gan:** Data curation. **Jie Ni:** Investigation. **Yunfeng Zhu:** Visualization. **Kaiting Cheng:** Project administration, Resources, Funding acquisition. **Lianhui Wang:** Project administration, Supervision, Funding acquisition.

Declaration of competing interest

The authors declare that they have no known competing financial interests or personal relationships that could have appeared to influence the work reported in this paper.

Acknowledgements

C.Y. Song, J.J. Zhang, J.R. Xiong, H.Y. Gan, J. Ni, Y.F. Zhu, L.H. Wang are supported by the National Key Research and Development Program of China (2017YFA0205300), National Natural Science Foundation of China (61871236), and Qinglan Project of Jiangsu Province of China. X.P. Miao, N. Chen, and K.T. Cheng are supported by the Emergency Key Program of Guangzhou Laboratory (EKPG21-10), Science and Technology Planning Project of Guangdong Province of China (2019B121205010), and Science and Technology Planning Project of Guangzhou of China (202008070005).

Appendix A. Supplementary data

Supplementary data to this article can be found online at https://doi.org/10.1016/j.bios.2022.114379.

References

Aydogdu, M.O., Rohn, J.L., Jafari, N.V., Brako, F., Homer-Vanniasinkam, S., Edirisinghe, M., 2022. Adv. Sci., e2104495
Bchetnia, M., Girard, C., Duchaine, C., Laprise, C., 2020. J. Infect. Public Health 13 (11), 1601–1610.
Bienko, M., Crosetto, N., Teytelman, L., Klemm, S., Itzkovitz, S., van Oudenaarden, A., 2013. Nat. Methods 10 (2), 122–124.
Chang, M.C., Hur, J., Park, D., 2020. Am. J. Phys. Med. Rehabil. 99 (7), 583–585.
Chen, Y., Liu, Q., Guo, D., 2020. J. Med. Virol. 92 (4), 418–423.
Cherkaoui, D., Huang, D., Miller, B.S., Turbe, V., McKendry, R.A., 2021. Biosens. Bioelectron. 189, 113328.
Corman, V.M., Landt, O., Kaiser, M., Molenkamp, R., Meijer, A., Chu, D.K., Bleicker, T., Brunink, S., Schneider, J., Schmidt, M.L., Mulders, D.G., Haagmans, B.L., van der Veer, B., van den Brink, S., Wijsman, L., Goderski, G., Romette, J.L., Ellis, J., Zambon, M., Peiris, M., Goossens, H., Reusken, C., Koopmans, M.P., Drosten, C., 2020. Euro Surveill. 25 (3), 2000045.
De Felice, M., De Falco, M., Zappi, D., Antonacci, A., Scognamiglio, V., 2022. Biosens. Bioelectron. 205, 114101.
Fan, Z., Yao, B., Ding, Y., Zhao, J., Xie, M., Zhang, K., 2021. Biosens. Bioelectron. 178, 113015.
Hossain, M.K., Kitahama, Y., Huang, G.G., Kaneko, T., Ozaki, Y., 2008. Appl. Phys. B 93 (1), 165–170.
Hwang, C., Park, N., Kim, E.S., Kim, M., Kim, S.D., Park, S., Kim, N.Y., Kim, J.H., 2021. Biosens. Bioelectron. 185, 113177.
Karami, A., Hasani, M., Azizi Jalilian, F., Ezati, R., 2021. Sensor. Actuator. B Chem. 328, 128971.
Klein, D., 2002. Trends Mol. Med. 8 (6), 257–260.
Lee, K., Drachev, V.P., Irudayaraj, J., 2011. ACS Nano 5 (3), 2109–2117.
Li, M., Yin, F., Song, L., Mao, X., Li, F., Fan, C., Zuo, X., Xia, Q., 2021. Chem. Rev. 121 (17), 10469–10558.
Liu, C., Zhou, Q., Li, Y., Garner, L.V., Watkins, S.P., Carter, L.J., Smoot, J., Gregg, A.C., Daniels, A.D., Jervey, S., Albaiu, D., 2020. ACS Cent. Sci. 6 (3), 315–331.
Liu, R., Zhang, S., Zheng, T.T., Chen, Y.R., Wu, J.T., Wu, Z.S., 2020. ACS Nano 14 (8), 9572–9584.
Mahapatra, S., Chandra, P., 2020. Biosens. Bioelectron. 165, 112361.
Mancuso, C.P., Lu, Z.X., Qian, J., Boswell, S.A., Springer, M., 2021. Anal. Chem. 93 (27), 9541–9548.
Markou, A., Tsaroucha, E.G., Kaklamanis, L., Fotinou, M., Georgoulias, V., Lianidou, E.S., 2008. Clin. Chem. 54 (10), 1696–1704.
Nguyen, H.A., Lee, N.Y., 2021. Biosens. Bioelectron. 189, 113353.
Nie, S., Emory, S.R., 1997. Science 275 (5303), 1102–1106.
Peng, H., Newbigging, A.M., Reid, M.S., Uppal, J.S., Xu, J., Zhang, H., Le, X.C., 2020. Anal. Chem. 92 (1), 292–308.
Perez-Lopez, B., Mir, M., 2021. Talanta 225, 121898.
Sharfstein, J.M., Becker, S.J., Mello, M.M., 2020. JAMA 323 (15), 1437–1438.
Sharma, B., Frontiera, R.R., Henry, A.I., Ringe, E., Van Duyne, R.P., 2012. Mater. Today 15 (1–2), 16–25.
Smyrlaki, I., Ekman, M., Lentini, A., Rufino de Sousa, N., Papanicolaou, N., Vondracek, M., Aarum, J., Safari, H., Muradrasoli, S., Rothfuchs, A.G., Albert, J., Hogberg, B., Reinius, B., 2020. Nat. Commun. 11 (1), 4812.
Sohrabi, C., Alsafi, Z., O'Neill, N., Khan, M., Kerwan, A., Al-Jabir, A., Iosifidis, C., Agha, R., 2020. Int. J. Surg. 76, 71–76.
Song, C., Chen, J., Zhao, Y., Wang, L., 2014. J. Mater. Chem. B 2 (43), 7488–7494.
Song, C., Jiang, X., Yang, Y., Zhang, J., Larson, S., Zhao, Y., Wang, L., 2020a. ACS Appl. Mater. Interfaces 12 (28), 31242–31254.

Song, C., Zhang, J., Liu, Y., Guo, X., Guo, Y., Jiang, X., Wang, L., 2020b. Sensor. Actuator. B Chem. 325, 128970.
Song, C.Y., Yang, Y.J., Yang, B.Y., Sun, Y.Z., Zhao, Y.P., Wang, L.H., 2016. Nanoscale 8 (39), 17365–17373.
Udugama, B., Kadhiresan, P., Kozlowski, H.N., Malekjahani, A., Osborne, M., Li, V.Y.C., Chen, H., Mubareka, S., Gubbay, J.B., Chan, W.C.W., 2020. ACS Nano 14 (4), 3822–3835.
Wang, M., Fu, A., Hu, B., Tong, Y., Liu, R., Liu, Z., Gu, J., Xiang, B., Liu, J., Jiang, W., Shen, G., Zhao, W., Men, D., Deng, Z., Yu, L., Wei, W., Li, Y., Liu, T., 2021. Small 17 (32), e2104078.
Wang, Y., Zheng, D., Tan, Q., Wang, M.X., Gu, L.Q., 2011. Nat. Nanotechnol. 6 (10), 668–674.
Wu, A., Peng, Y., Huang, B., Ding, X., Wang, X., Niu, P., Meng, J., Zhu, Z., Zhang, Z., Wang, J., Sheng, J., Quan, L., Xia, Z., Tan, W., Cheng, G., Jiang, T., 2020. Cell Host Microbe 27 (3), 325–328.
Wu, F., Zhao, S., Yu, B., Chen, Y.M., Wang, W., Song, Z.G., Hu, Y., Tao, Z.W., Tian, J.H., Pei, Y.Y., Yuan, M.L., Zhang, Y.L., Dai, F.H., Liu, Y., Wang, Q.M., Zheng, J.J., Xu, L., Holmes, E.C., Zhang, Y.Z., 2020. Nature 579 (7798), 265–269.
Wu, Y., Fu, C., Shi, W., Chen, J., 2021. Talanta 235, 122735.
Yang, Y., Song, C., Zhang, J., Chao, J., Luong, H.M., Zhao, Y., Wang, L., 2022. Nanoscale 14 (12), 4538–4547.
Yin, K., Ding, X., Xu, Z., Li, Z., Wang, X., Zhao, H., Otis, C., Li, B., Liu, C., 2021. Sensor. Actuator. B Chem. 344, 130242.
Yin, P., Choi, H.M., Calvert, C.R., Pierce, N.A., 2008. Nature 451 (7176), 318–322.
Zhang, J., Yang, Y., Jiang, X., Dong, C., Song, C., Han, C., Wang, L., 2019. Biosens. Bioelectron. 141, 111402.
Zhu, X., Wang, X., Han, L., Chen, T., Wang, L., Li, H., Li, S., He, L., Fu, X., Chen, S., Xing, M., Chen, H., Wang, Y., 2020. Biosens. Bioelectron. 166, 112437.